The Numerical Analysis of Spindle Motor Bearing Composed of Herringbone Groove Journal and Spiral Groove Thrust Bearing

Sang-Man Oh and Yoon-Chul Rhim†

Graduate School, Yonsei University
School of Electrical & Mechanical Eng., Yonsei University

Abstract : Ball bearings have been widely used for the spindle motor bearing in various kinds of information storage devices. Recently many researchers have been trying to replace ball bearings with fluid film bearings because of their superior NRRO(non-repeatable runout) characteristics. In this study, a numerical analysis has been conducted for the complicate bearing system composed of herringbone groove journal bearing and spiral groove thrust bearing for the spindle motor of the information storage device. At first, spindle motor bearing is modeled as journal bearing part and thrust bearing part separately, and then observed various influences of geometric parameters. Previous studies had considered only the translational motion of the journal bearing. However, this study takes the additional 2-degree of freedom rotation into consideration to attempt to describe the real motion of the spindle bearing. As a result, rotational stiffness coefficients and rotational damping coefficients are obtained. In addition, a spindle bearing system made up of four bearings is modeled and interpreted at once and coefficients of dynamic characteristics of each bearing are obtained. Finally, an eigen analysis of bearing system is made with these results. Through this analysis, it is possible to estimate an unstable condition of the system for given geometric parameters and to propose a method which is able to avoid the unstable condition by a proper adjustment of geometric parameters.

Keywords : Fluid film spindle motor bearing, herringbone groove journal bearing, spiral groove thrust bearing, conical motion, eigen analysis, stability, perturbation method, finite difference method

Introduction

The storage density of information storage device such as hard-disk drive can be represented by bits per inch (BPI) and track per inch (TPI), which have been increased continuously in the last decade. Storage capacity also has been astonishingly increased and it seems that it will continue increasing for some time. Moreover the demand for the information storage device of high capacity increases without break. It is necessary to increase rotational speed and TPI to make the information storage device higher capacity. At present the rotational speed of the spindle motor for the hard disk drive is already over 10,000 rpm and TPI also exceeds 34,000.

We have used ball bearings in the spindle motor of the hard disk drive, whose critical defects is the non-repeatable runout (NRRO) due to the geometric error. The diminution of NRRO is necessary for the accomplishment of large number of TPI and high degree of reliability of reading and writing performance. However, it seems quite difficult to make the ball bearing of desired specification for the time being owing to the limits of accurate manufacturing, and making the small bearing balls for the small size spindle motor is extremely difficult. Therefore, there have been researches for the method of

substituting the fluid film bearing for the ball bearing. This method can diminish the room for bearing in the motor, enable non-contact rotation, increase damping of the spindle so as to reduce NRRO, bring enhanced vibration-and-shock-absorbing ability, and decrease the noise level of the spindle system especially at high speed region.

Fluid film bearing is generally divided into two groups, one is to use gas and the other is to use oil. Gas-lubricated fluid film bearing is free of pollution and goes well with the environment but it seems difficult to have the stiffness like ball bearing. On the other hand, oil-lubricated fluid film bearing has enough stiffness to substitute ball bearing. But plain journal bearing has inherent instability characteristics at lightly-loaded condition such as high-speed rotation or vertical rotation with small eccentricity ratio. To overcome this defect grooves are processed on the bearing surface so that stable whirl motion is obtained with non-zero stiffness at concentric condition. However, oil-lubricated fluid film bearing has some issues to solve for the adoption to the spindle motor bearing. For instance, it is difficult to predict characteristics change of the oil at the small length scale (μm) of the design tolerance, the clearance of bearing, the surface roughness, and the capillary sealing. Furthermore, journal and thrust bearing should be fixed up in parallel and perpendicular position, and it is not easy to generate precise grooves. Proper selection of the lubricant is also a problem. Besides, high-speed rotation,

†Corresponding author; Tel: 82-2-2123-2820, Fax: 82-2-364-0896
E-mail: rhimyc@yonsei.ac.kr

prevention of leakage, repeatable start-stop motion, reliable life, and adequate stiffness to shock and vibration should be considered together.

In general, oil-lubricated fluid film bearing for the hard disk drive spindle is composed of two journal bearings (upper/ lower) and both-sided thrust bearings or top and bottom sided thrust bearings. Grooves are processed on the bearing surface to pump oil according to the rotation so that bearings can support the rotor with generated pressure even at the concentric condition. And grooves of journal bearing should be properly adjusted to pump sufficient oil to upper thrust bearing.

In the latter half of 80s, it turned out that NGT was not suitable for the case of finite number of grooves. So Bonneau and Absi solved compressible Reynolds equation to get stiffness and damping coefficients by finite element method [1]. Kang et al. analyzed dynamic characteristics of oil-lubricated groove journal bearing for the case of 8 grooves [2], Qiu et al. studied misalignment effect of hydrodynamic journal bearing [3].

Zang and Hatch split the spindle bearing into journal and thrust part, solved separately with the convergence of mass flow, tried the simplified analysis of whirl characteristics [4,5]. Rahman, Leuthold conducted finite element analysis with full Sommerfeld boundary condition [6]. Zhu, Ono compared several kinds of thrust bearings for the spindle motor bearing [7], Jang and Kim presented how to calculate the dynamic coefficients of fluid film bearing considering the 5 degree of freedom motion [8].

At present hard disk drive with hydrodynamic spindle bearing has come out into the market, but it has been developed for low noise point of view. Inferring from the current tendency of high capacity, miniaturization and power saving, fluid film bearing has room for development.

In this study, a numerical simulation is coded for the spindle motor bearing composed of two herringbone groove journal bearings and two spiral groove thrust bearings for HDD. Oil is used as a lubricant, so the incompressible Reynolds equation is
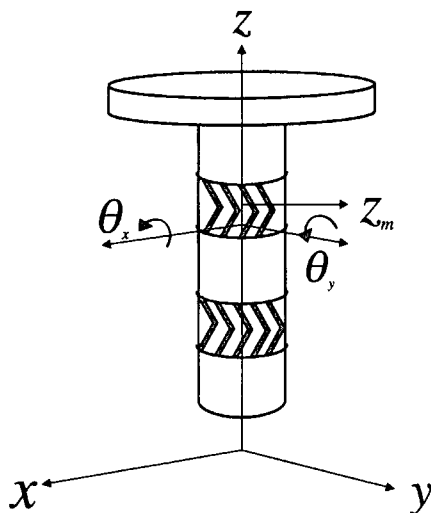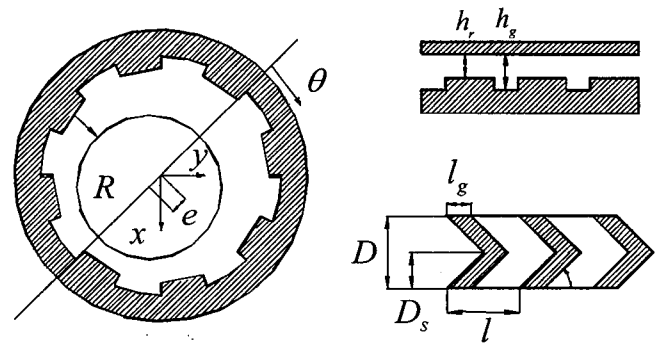

Fig. 2. Schematic of Herringbone groove journal bearing with rectangular-profile grooves and definitions of bearing parameters (groove depth ratio for concentric position ($\Gamma=h_g/h_r$), groove width ratio ($\alpha=l_g/l$), and groove angle (β)).
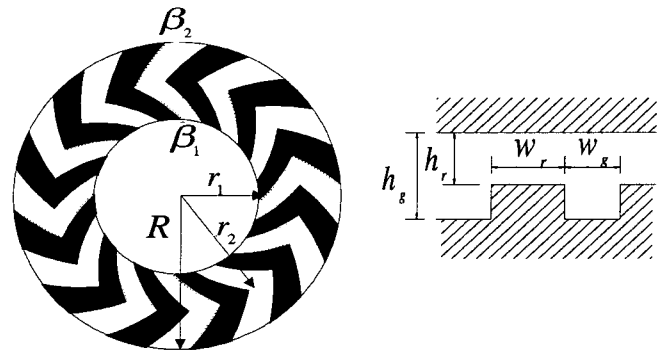

Fig. 3. Schematic of spiral groove thrust bearing with rectangular-profile grooves and definitions of bearing parameters (groove depth ratio($\Gamma=h_g/h_r$), groove width ratio($\alpha=w_g/(w_r+w_g)$), and spiral angle(β)).

solved. Optimal geometries of bearings are investigated. Figure 1 shows schematic diagram and coordinates of the spindle motor bearing. Figure 2 shows the geometry of herringbone groove journal bearing and design parameters.

Actual motion of spindle motor bearing is made up of translational motions in x, y, z-direction and rotational motions in θ_x, θ_y-direction. Rotational motions had not been considered in previous researches but they are not negligible in practical run and seem to influence largely on stability of the whole system. Figure 4 shows 5-degree of freedom motions of spindle motor bearing.

Whole bearing system can be simulated by gathering the codes that computes bearing characteristics separately. Design parameters can be fixed for the spindle motor bearing from the stored data of coupled dynamic characteristics. So stiffness and damping coefficients of the spindle motor bearing calculated with recommendable geometrical parameters of journal and thrust bearing. Then stability of the spindle bearing is investigated considering high speed rotation beyond 10,000 rpm.

Integrating the results above, propriety of using herringbone groove journal and thrust bearing as a spindle motor bearing for the HDD is examined, and the reliable values can be suggested for practical design.
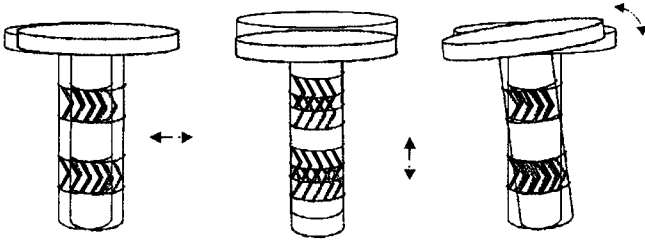

Fig. 1. Geometry and coordinate system of the spindle motor bearing.

Fig. 4. 5-degree of freedom motion of the spindle motor bearing.

Analysis of Journal and Thrust Bearing

Governing equation for journal bearing

The pressure distribution in a fluid film bearing can be computed by the Reynolds equation which is derived from the Navier-Stokes equations.

$$\frac{\partial}{\partial x}\left(\frac{h^3}{12\mu}\frac{\partial p}{\partial x}\right) + \frac{\partial}{\partial z}\left(\frac{h^3}{12\mu}\frac{\partial p}{\partial z}\right) = \frac{1}{2}\left[\frac{\partial(uh)}{\partial x} + \frac{\partial(wh)}{\partial z}\right] + \frac{\partial h}{\partial t}$$

(2.1)

Where, x and z direction represent the circumferential and axial direction, respectively.

Since there is no axial motion in steady state, the axial velocity w is zero, actually. Once above equation is solved with appropriate boundary conditions we can get the two-dimensional pressure distribution, flow rates in each direction, and friction.

Reynolds equation is transformed in cylindrical coordinate for the analysis of the journal bearing in Eqn. (2.2).

$$\frac{1}{R^2}\frac{\partial}{\partial\theta}\left(\frac{h^3}{12\mu_0}\frac{\partial p}{\partial\theta}\right) + \frac{\partial}{\partial z}\left(\frac{h^3}{12\mu_0}\frac{\partial p}{\partial z}\right) = \frac{\omega}{2}\frac{\partial h}{\partial\theta} + \frac{\partial h}{\partial t}$$

(2.2)

Boundary conditions for this problem are the pressure at both ends in axial direction is set to be the ambient pressure, i.e. zero and periodic in circumferential direction. Reynolds boundary condition is applied to the area in which cavitation occurs. In mathematical expression,

$$p = p_a \quad \text{at} \quad z = 0, L$$
$$p(\theta) = p(\theta + 2\pi)$$

(2.3)

$$\frac{\partial p}{\partial\theta} = 0 \quad \text{at} \quad p \leq p_a$$

Herringbone groove journal bearing has couples of chevron grooves on journal surface, as shown in Fig. 5. It is convenient to transform the oblique physical domain to the orthogonal computational domain. The transformation is done as follows.

$$for \quad -\lambda \leq z \leq 0 \qquad -\lambda \leq \xi \leq 0 \qquad (2.4)$$
$$z = \xi \qquad\qquad \xi = z$$

$$\theta = 2\pi\eta - \frac{L}{R}\cot\beta_1\xi \quad \eta = \left(\theta + \frac{L}{R}\cot\beta_1\xi\right)/2\pi$$
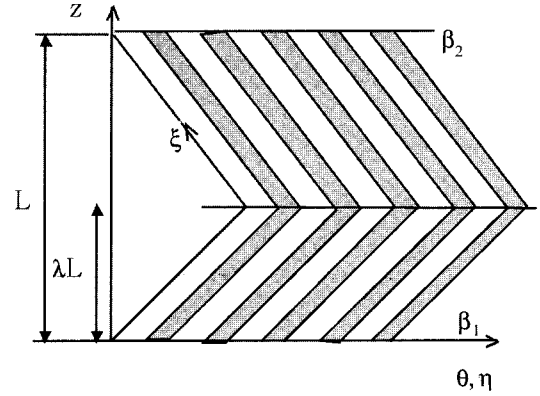
Transformation for journal bearing

Fig. 5. Transformation for HGJB.

$$for \quad 0 \leq z \leq 1-\lambda \qquad 0 \leq \xi \leq 1-\lambda$$
$$z = \xi \qquad\qquad \xi = z \qquad\qquad (2.5)$$

$$\theta = 2\pi\eta - \frac{L}{R}\cot\beta_2\xi \quad \eta = \left(\theta + \frac{L}{R}\cot\beta_2\xi\right)/2\pi$$

The transformed Reynolds equation is obtained using the transformation rules as follows.

$$\frac{\partial}{\partial\theta} = \frac{\partial}{\partial\xi}\frac{\partial\xi}{\partial\theta} + \frac{\partial}{\partial\eta}\frac{\partial\eta}{\partial\theta} = \frac{1}{2\pi}\frac{\partial}{\partial\eta}$$

$$\frac{\partial}{\partial z} = \frac{\partial}{\partial\xi}\frac{\partial\xi}{\partial z} + \frac{\partial}{\partial\eta}\frac{\partial\eta}{\partial z} = \frac{\partial}{\partial\xi} + \frac{L\cot\beta}{2\pi R}\frac{\partial}{\partial\eta}$$

(2.6)

Calculation of dynamic coefficients for journal bearing

To obtain dynamic coefficients of the journal bearing, perturbed pressure due to the small amplitude motion of the journal bearing is taken by the perturbation method.

When the journal bearing moves with the small amplitude motion (Δx, Δy, $\Delta\theta_x$, $\Delta\theta_y$, $\Delta\dot{x}$, $\Delta\dot{y}$, $\Delta\dot{\theta}_x$, $\Delta\dot{\theta}_y$), first-order expansion of fluid film is as follows.

$$h = h_0 + (\Delta x + z'\Delta\theta_y)\cos\theta' + (\Delta y - z'\Delta\theta_x)\sin\theta'$$
(2.7)
$$\frac{dh}{dt} = (\Delta\dot{x} + z'\Delta\dot{\theta}_y)\cos\theta' + (\Delta\dot{y} - z'\Delta\dot{\theta}_x)\sin\theta'$$

Similarly, the change of pressure distribution in fluid film for small amplitude motion can be obtained by a first-order expansion:

$$p = p_0 + \left(\frac{\partial p}{\partial x}\right)_0\Delta x + \left(\frac{\partial p}{\partial y}\right)_0\Delta y + \left(\frac{\partial p}{\partial\theta_x}\right)_0\Delta\theta_x + \left(\frac{\partial p}{\partial\theta_y}\right)_0\Delta\theta_y$$

$$+ \left(\frac{\partial p}{\partial\dot{x}}\right)_0\Delta\dot{x} + \left(\frac{\partial p}{\partial\dot{y}}\right)_0\Delta\dot{y} + \left(\frac{\partial p}{\partial\dot{\theta}_x}\right)_0\Delta\dot{\theta}_x + \left(\frac{\partial p}{\partial\dot{\theta}_y}\right)_0\Delta\dot{\theta}_y$$

(2.8)

Derivatives will be expressed as follows for convenience.

$$(p)_0 = p_0 \quad \left(\frac{\partial p}{\partial x}\right)_0 = p_x \quad \left(\frac{\partial p}{\partial y}\right)_0 = p_y \quad \left(\frac{\partial p}{\partial\dot{x}}\right)_0 = p_{\dot{x}}$$

$$\left(\frac{\partial p}{\partial \dot{y}}\right)_0 = p_{\dot{y}} \quad \left(\frac{\partial p}{\partial \theta_x}\right)_0 = p_{\theta_x} \quad \left(\frac{\partial p}{\partial \theta_y}\right)_0 = p_{\theta_y} \quad (2.9)$$

$$\left(\frac{\partial p}{\partial \dot{\theta}_x}\right)_0 = p_{\dot{\theta}_x} \quad \left(\frac{\partial p}{\partial \dot{\theta}_y}\right)_0 = p_{\dot{\theta}_y}$$

Substituting Eqn. (2.7), (2.8) into Eqn. (2.2) retaining only the first order terms and separating into $O(1)$, $O(\Delta x)$, $O(\Delta y)$, $O(\Delta\theta_x)$, $O(\Delta\theta_y)$, $O(\Delta\dot{x})$, $O(\Delta\dot{y})$, $O(\Delta\dot{\theta}_x)$, and $O(\Delta\dot{\theta}_y)$, nine perturbation equations are obtained:

$$\left[\frac{1}{R^2}\frac{\partial}{\partial\theta'}\left(\frac{h^3}{12\mu}\frac{\partial}{\partial\theta'}\right) + \frac{\partial}{\partial z}\left(\frac{h^3}{12\mu}\frac{\partial}{\partial z}\right)\right]\begin{Bmatrix} p_0 \\ p_x \\ p_y \\ p_{\dot{x}} \\ p_{\dot{y}} \end{Bmatrix} = \begin{Bmatrix} \dfrac{\omega}{2}\dfrac{\partial h_0}{\partial\theta} \\[2mm] -\dfrac{\omega}{2}\left(\sin\theta' + \dfrac{3\cos\theta'}{h_0}\dfrac{\partial h_0}{\partial\theta}\right) \\[1mm] -\dfrac{h_0}{4\mu}\left[\dfrac{1}{R^2}\dfrac{\partial p_0}{\partial\theta'}\dfrac{\partial}{\partial\theta'}\left(\dfrac{\cos\theta'}{h_0}\right) + \dfrac{\partial p_0}{\partial z}\dfrac{\partial}{\partial z}\left(\dfrac{\cos\theta'}{h_0}\right)\right] \\[2mm] \dfrac{\omega}{2}\left(\cos\theta' + \dfrac{3\sin\theta'}{h_0}\dfrac{\partial h_0}{\partial\theta}\right) \\[1mm] -\dfrac{h_0}{4\mu}\left[\dfrac{1}{R^2}\dfrac{\partial p_0}{\partial\theta'}\dfrac{\partial}{\partial\theta'}\left(\dfrac{\sin\theta'}{h_0}\right) + \dfrac{\partial p_0}{\partial z}\dfrac{\partial}{\partial z}\left(\dfrac{\sin\theta'}{h_0}\right)\right] \\[2mm] \cos\theta' \\[1mm] \sin\theta' \end{Bmatrix} \quad (2.10)$$

$$\left[\frac{1}{R^2}\frac{\partial}{\partial\theta'}\left(\frac{h^3}{12\mu}\frac{\partial}{\partial\theta'}\right) + \frac{\partial}{\partial z}\left(\frac{h^3}{12\mu}\frac{\partial}{\partial z}\right)\right]\begin{Bmatrix} p_{\theta_x} \\ p_{\theta_y} \\ p_{\dot{\theta}_x} \\ p_{\dot{\theta}_y} \end{Bmatrix} = \begin{Bmatrix} z'\left[\begin{array}{c} -\dfrac{\omega}{2}\left(\cos\theta' + \dfrac{3\sin\theta'}{h_0}\dfrac{\partial h_0}{\partial\theta}\right) \\[1mm] -\dfrac{h_0}{4\mu}\left[\dfrac{1}{R^2}\dfrac{\partial p_0}{\partial\theta'}\dfrac{\partial}{\partial\theta'}\left(\dfrac{\sin\theta'}{h_0}\right) + \dfrac{\partial p_0}{\partial z}\dfrac{\partial}{\partial z}\left(\dfrac{\sin\theta'}{h_0}\right)\right] \end{array}\right] \\[1mm] +\dfrac{\partial z'}{\partial z}\left(\dfrac{h_0^2}{4\mu}\sin\theta'\dfrac{\partial p_0}{\partial z}\right) \\[3mm] z'\left[\begin{array}{c} -\dfrac{\omega}{2}\left(\sin\theta' + \dfrac{3\cos\theta'}{h_0}\dfrac{\partial h_0}{\partial\theta}\right) \\[1mm] -\dfrac{h_0}{4\mu}\left[\dfrac{1}{R^2}\dfrac{\partial p_0}{\partial\theta'}\dfrac{\partial}{\partial\theta'}\left(\dfrac{\cos\theta'}{h_0}\right) + \dfrac{\partial p_0}{\partial z}\dfrac{\partial}{\partial z}\left(\dfrac{\cos\theta'}{h_0}\right)\right] \end{array}\right] \\[1mm] -\dfrac{\partial z'}{\partial z}\left(\dfrac{h_0^2}{4\mu}\cos\theta'\dfrac{\partial p_0}{\partial z}\right) \\[3mm] -z'\sin\theta' \\[2mm] z'\cos\theta' \end{Bmatrix} \quad (2.11)$$

Bearing reaction forces and moments as well as load carrying capacity can be determined by integrating the solutions in the bearing area.

$$\begin{Bmatrix} F_x \\ F_y \\ M_{\theta_x} \\ M_{\theta_y} \end{Bmatrix} = \{F_0\} + [K]\begin{Bmatrix} \Delta x \\ \Delta y \\ \Delta\theta_x \\ \Delta\theta_y \end{Bmatrix} + [C]\begin{Bmatrix} \Delta\dot{x} \\ \Delta\dot{y} \\ \Delta\dot{\theta}_x \\ \Delta\dot{\theta}_y \end{Bmatrix} \quad (2.12)$$

$$\{F_0\} = \begin{Bmatrix} F_{x0} \\ F_{y0} \\ M_{\theta_x 0} \\ M_{\theta_y 0} \end{Bmatrix} = \iint_{\theta z} \begin{Bmatrix} -p_0\cos\theta' \\ -p_0\sin\theta' \\ z'p_0\sin\theta' \\ -z'p_0\cos\theta' \end{Bmatrix} r_1 d\theta dz$$

where, $\{F_0\}$, $[K]$, and $[C]$ are load carrying capacity, stiffness and damping matrix, respectively, and they can be represented as following:
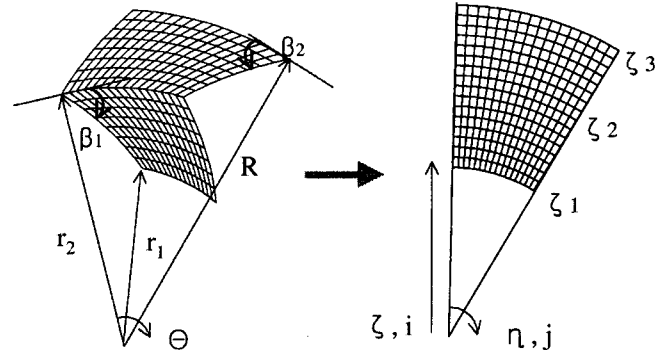

Fig. 6. Transformation for logarithmic spiral groove.

$$[K] = \begin{Bmatrix} K_{xx} & K_{xy} & K_{x\theta_x} & K_{x\theta_y} \\ K_{yx} & K_{yy} & K_{y\theta_x} & K_{y\theta_y} \\ K_{\theta_x x} & K_{\theta_x y} & K_{\theta_x \theta_x} & K_{\theta_x \theta_y} \\ K_{\theta_y x} & K_{\theta_y y} & K_{\theta_y \theta_x} & K_{\theta_y \theta_y} \end{Bmatrix} = \iint_{\theta z} \begin{Bmatrix} -\cos\theta' \\ -\sin\theta' \\ z'\sin\theta' \\ -z'\cos\theta' \end{Bmatrix} \{p_x \;\; p_y \;\; p_{\theta_x} \;\; p_{\theta_y}\} r_1 d\theta dz$$

$$[C] = \begin{Bmatrix} C_{xx} & C_{xy} & C_{x\theta_x} & C_{x\theta_y} \\ C_{yx} & C_{yy} & C_{y\theta_x} & C_{y\theta_y} \\ C_{\theta_x x} & C_{\theta_x y} & C_{\theta_x \theta_x} & C_{\theta_x \theta_y} \\ C_{\theta_y x} & C_{\theta_y y} & C_{\theta_y \theta_x} & C_{\theta_y \theta_y} \end{Bmatrix} = \iint_{\theta z} \begin{Bmatrix} -\cos\theta' \\ -\sin\theta' \\ z'\sin\theta' \\ -z'\cos\theta' \end{Bmatrix} \{p_{\dot{x}} \;\; p_{\dot{y}} \;\; p_{\dot{\theta}_x} \;\; p_{\dot{\theta}_y}\} r_1 d\theta dz$$

Transformation of thrust bearing

The suitable transformation of thrust bearing is necessary, since groove goes along with logarithmic spiral.
Logarithmic spiral is expressed as following.

$$r = r_0 e^{-\tan\beta\theta} = r_0 e^{m\theta} \qquad \theta = \frac{1}{m}\log\frac{r}{r_0} \tag{2.13}$$

Transformation is conducted into two separate regions as following.

$r_1 \le r \le r_2 \qquad\qquad r_2 \le r \le R$

$\xi = r \qquad\qquad\qquad \xi = r$

$$\eta = \theta - \frac{1}{m_1}\log\frac{r}{R} \qquad \eta = \theta - \frac{1}{m_1}\log\frac{r_2}{R} + \frac{1}{m_2}\log\frac{r_2}{R} - \frac{1}{m_2}\log\frac{r}{R} \tag{2.14}$$

$\xi_1 \le \xi \le \xi_2 \qquad\qquad \xi_2 \le \xi \le \xi_3$

$r = \xi \qquad\qquad\qquad r = \xi$

$$\eta = \theta - \frac{1}{m_1}\log\frac{\xi}{R} \qquad \eta = \theta - \frac{1}{m_1}\log\frac{\xi_2}{R} + \frac{1}{m_2}\log\frac{\xi_2}{R} - \frac{1}{m_2}\log\frac{\xi}{R} \tag{2.15}$$

The transformed Reynolds equation is obtained using the transformation rules as follows.

for $\xi_1 \le \xi \le \xi_2$ $\qquad\qquad\qquad$ for $\xi_2 \le \xi \le \xi_3$

$$\frac{\partial}{\partial r} = \frac{\partial}{\partial \xi}\frac{\partial \xi}{\partial r} + \frac{\partial}{\partial \eta}\frac{\partial \eta}{\partial r} = \frac{\partial}{\partial \xi} - \frac{1}{m_1 \xi}\frac{\partial}{\partial \eta} \qquad \frac{\partial}{\partial r} = \frac{\partial}{\partial \xi}\frac{\partial \xi}{\partial r} + \frac{\partial}{\partial \eta}\frac{\partial \eta}{\partial r} = \frac{\partial}{\partial \xi} - \frac{1}{m_2 \xi}\frac{\partial}{\partial \eta}$$

$$\frac{\partial}{\partial \theta} = \frac{\partial}{\partial \xi}\frac{\partial \xi}{\partial \theta} + \frac{\partial}{\partial \eta}\frac{\partial \eta}{\partial \theta} = \frac{\partial}{\partial \eta} \qquad\qquad \frac{\partial}{\partial \theta} = \frac{\partial}{\partial \xi}\frac{\partial \xi}{\partial \theta} + \frac{\partial}{\partial \eta}\frac{\partial \eta}{\partial \theta} = \frac{\partial}{\partial \eta} \tag{2.16}$$

Steady-state solution of thrust bearing

To analyze the thrust bearing, the Reynolds equation in polar coordinate is adopted as following:

$$\frac{\partial}{\partial r}\left(rh^3\frac{\partial p}{\partial r}\right)+\frac{1}{r}\frac{\partial}{\partial \theta}\left(h^3\frac{\partial p}{\partial \theta}\right) = 6\mu\omega r\frac{\partial h}{\partial \theta}+12\mu r\frac{\partial h}{\partial t} \quad (2.17)$$

The boundary condition is specified at the inner and outer radius as ambient pressure, and periodic conditions for circumferential direction. And the Reynolds boundary condition is applied for the cavitation region. These are as following:

$$p = p_a \quad at \quad r = r_1, r_2$$
$$p(\theta) = p(\theta + 2\pi) \quad\quad\quad\quad\quad (2.18)$$

$$\frac{\partial p}{\partial \theta} = 0 \quad at \quad p \leq p_a$$

Calculation of dynamic coefficients for thrust bearing

When the thrust bearing wobbles with small amplitude (Δz, $\Delta\theta_x$, $\Delta\theta_y$, $\Delta\dot{z}$, $\Delta\dot{\theta}_x$, $\Delta\dot{\theta}_y$), the first-order expansion of the fluid film and the change of pressure distribution are as following:

$$h = h_0 + r(-\Delta\theta_x\sin\theta + \Delta\theta_y\cos\theta) + \Delta z$$

$$\frac{dh}{dt} = r(\Delta\dot{\theta}_x sin\theta' + \dot{\theta}_y cos\theta') + \Delta\dot{z} \quad\quad (2.19)$$

$$p = p_0 + \Delta z p_z + \Delta\dot{z}\dot{p}_z + \Delta\theta_x p_{\theta_x} + \Delta\theta_y p_{\theta_y} + \Delta\theta_x\dot{p}_{\theta_x} + \Delta\theta_x\dot{p}_{\theta_x}$$

Substituting Eqn. (3.7) into Eqn. (3.5) retaining only the first order terms and separating into $O(1)$, $O(\Delta z)$, $O(\Delta\theta_x)$, $O(\Delta\theta_y)$, $O(\Delta\dot{z})$, $O(\Delta\dot{\theta}_x)$, and $O(\Delta\dot{\theta}_y)$, seven perturbed equations are obtained:

$$\left[\frac{\partial}{\partial r}\left(rh^3\frac{\partial}{\partial r}\right)+\frac{1}{r}\frac{\partial}{\partial \theta}\left(h^3\frac{\partial}{\partial \theta}\right)\right]\begin{Bmatrix}p_0\\p_z\\p_z\\p_{\theta_x}\\p_{\theta_y}\\p_{\theta_x}\\p_{\theta_y}\end{Bmatrix} = \begin{pmatrix}6\mu\omega r\dfrac{\partial h}{\partial \theta}\\[6pt]-\dfrac{\partial}{\partial r}\left(3rh_0^3\dfrac{\partial p_0}{\partial r}\right)-\dfrac{1}{r}\dfrac{\partial}{\partial \theta}\left(3h_0^3\dfrac{\partial p_0}{\partial \theta}\right)\\[6pt]12\mu r\\[6pt]\begin{pmatrix}\sin\theta'\left[3\dfrac{r}{h_0}\dfrac{\partial h_0}{\partial \theta}-3rh_0\dfrac{\partial h_0}{\partial r}\dfrac{\partial p_0}{\partial r}-3\dfrac{h_0}{r}\dfrac{\partial h_0}{\partial \theta}\dfrac{\partial p_0}{\partial \theta}\right]\\+3h_0^2\sin\theta'\dfrac{\partial p_0}{\partial r}+3\dfrac{h_0}{r}\cos\theta'\dfrac{\partial p_0}{\partial \theta}-r\cos\theta'\end{pmatrix}\\[6pt]\begin{pmatrix}-\cos\theta'\left[3\dfrac{r}{h_0}\dfrac{\partial h_0}{\partial \theta}-3rh_0\dfrac{\partial h_0}{\partial r}\dfrac{\partial p_0}{\partial r}-3\dfrac{h_0}{r}\dfrac{\partial h_0}{\partial \theta}\dfrac{\partial p_0}{\partial \theta}\right]\\-3h_0^2\cos\theta'\dfrac{\partial p_0}{\partial r}+3\dfrac{h_0}{r}\sin\theta'\dfrac{\partial p_0}{\partial \theta}-r\sin\theta'\end{pmatrix}\\[6pt]-r\sin\theta'\\[4pt]r\cos\theta'\end{pmatrix} \quad (2.20)$$

Bearing reaction forces and moments as well as load carrying capacity can be determined by integrating the solutions for the bearing area.

$$\begin{Bmatrix}F_z\\M_{\theta_x}\\M_{\theta_y}\end{Bmatrix} = \{F_0\}+[K]\begin{Bmatrix}\Delta z\\\Delta\theta_x\\\Delta\theta_y\end{Bmatrix}+[C]\begin{Bmatrix}\Delta z\\\Delta\theta_x\\\Delta\theta_y\end{Bmatrix} \quad\quad (2.21)$$

where, $\{F_0\}$, $[K]$, and $[C]$ are load carrying capacity, stiffness and damping matrix, respectively, and they can be represented as following:

$$\{F_0\} = \begin{Bmatrix}F_{z0}\\M_{\theta_x 0}\\M_{\theta_y 0}\end{Bmatrix} = \iint_{r\theta}\begin{Bmatrix}-p_0\\p_0\sin\theta'\\-p_0\cos\theta'\end{Bmatrix}rdrd\theta$$

$$[K] = \begin{Bmatrix} \begin{bmatrix} K_{zz} & K_{z\theta_x} & K_{z\theta_y} \\ K_{\theta_{x}z} & K_{\theta_{x}\theta_{x}} & K_{\theta_{x}\theta_{y}} \\ K_{\theta_{y}z} & K_{\theta_{y}\theta_{x}} & K_{\theta_{y}\theta_{y}} \end{bmatrix} \end{Bmatrix} = \iint_{r\theta} \begin{Bmatrix} -1 \\ r\sin\theta' \\ -r\sin\theta' \end{Bmatrix} \{p_z \quad p_{\theta_x} \quad p_{\theta_y}\} r\,dr\,d\theta$$

$$[C] = \begin{Bmatrix} \begin{bmatrix} C_{zz} & C_{z\theta_x} & C_{z\theta_y} \\ C_{\theta_{x}z} & C_{\theta_{x}\theta_{x}} & C_{\theta_{x}\theta_{y}} \\ C_{\theta_{y}z} & C_{\theta_{y}\theta_{x}} & C_{\theta_{y}\theta_{y}} \end{bmatrix} \end{Bmatrix} = \iint_{r\theta} \begin{Bmatrix} -1 \\ r\sin\theta' \\ -r\sin\theta' \end{Bmatrix} \{p_{\dot{z}} \quad p_{\dot{\theta}_x} \quad p_{\dot{\theta}_y}\} r\,dr\,d\theta$$

Finite difference method

The governing equation is a kind of Poisson equation. There are couple of solution methods for the elliptic partial differential equation such as Poisson equation. The most powerful and simple method is alternating direction implicit (ADI) method which uses tri-diagonal matrix solver in two principal directions. And optimization of relaxation factor can make convergence fast.

The convergence error is the ratio of absolute sum of pressure change by iteration to absolute sum of pressure itself.

$$\frac{\Sigma |P_{I,J}^{new} - P_{I,J}^{old}|}{\Sigma |P_{I,J}^{new}|} < 10^{-5} \qquad (2.21)$$

Analysis of Spindle Motor Bearing

Static and dynamic characteristics of spindle bearing

Analyzed models previously done in Chapter2 and 3 are integrated to solve the whole spindle bearing system. Spindle bearing consists of journal bearing #1, #2, thrust bearing #1, #2, and oil resorviers between bearings, and all parts is connected by the boundary condition that mass flow through the boundary is conserved. Oil resorvier is considered as a plain journal bearing with very larger clearance compared to the herringbone groove journal bearing.

Boundary condition between journal bearing and oil reservoir is as following:

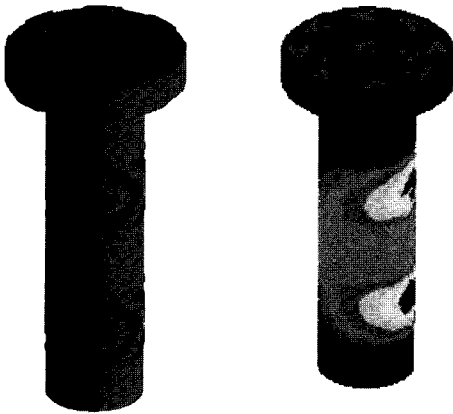$$(q_z)_{journal} = (q_z)_{oil \ reservior} \qquad (3.1)$$

Fig. 7. Gap and pressure profiles of the spindle motor bearing.

Boundary condition between thrust bearing and oil reservoir is as following:

$$(q_r)_{thrust} = (q_z)_{oil \ reservior} \qquad (3.2)$$

Axial and radial flow are obtained from the flow equation.

$$q_r = -\frac{h^3}{12\mu}\frac{\partial p}{\partial r} \qquad (3.3)$$

$$q_z = -\frac{h^3}{12\mu}\frac{\partial p}{\partial z} \qquad (3.4)$$

Substituting Eqn. (3.3) and (3.4) into Eqn. (3.1) and (3.2), boundaries between journal bearing, thrust bearing and oil resorviers are included in calculation.

Fig. 7 shows the gap and pressure profiles of the spindle motor bearing as a whole.

Eigen analysis of system

Considering translational motion in x,y-direction and rotational motion in θ_x, θ_y-direction, the linearized dynamic equation of journal is as Eqn. (2.12).

Assuming that no external force is applied to the system with the steady-state conditions, Eqn. (2.12) will be recast as following:
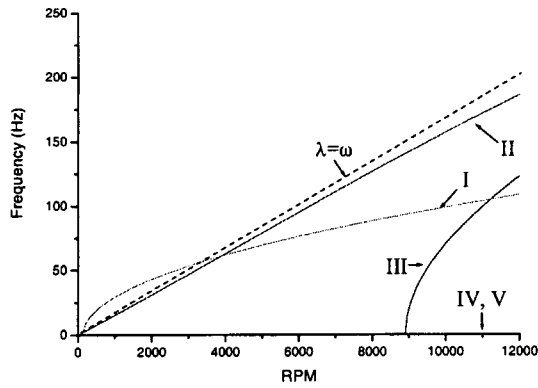
$$\begin{pmatrix} M & 0 & 0 & 0 \\ 0 & M & 0 & 0 \\ 0 & 0 & I_{xx} & 0 \\ 0 & 0 & 0 & I_{yy} \end{pmatrix}\begin{Bmatrix} \Delta\ddot{x} \\ \Delta\ddot{y} \\ \Delta\ddot{\theta}_x \\ \Delta\ddot{\theta}_y \end{Bmatrix} + \begin{bmatrix} C_{xx} & C_{xy} & C_{x\theta_x} & C_{x\theta_y} \\ C_{yx} & C_{yy} & C_{y\theta_x} & C_{y\theta_y} \\ C_{\theta_{x}x} & C_{\theta_{x}y} & C_{\theta_{x}\theta_{x}} & C_{\theta_{x}\theta_{y}} \\ C_{\theta_{y}x} & C_{\theta_{y}y} & C_{\theta_{y}\theta_{x}} & C_{\theta_{y}\theta_{y}} \end{bmatrix}\begin{Bmatrix} \Delta\dot{x} \\ \Delta\dot{y} \\ \Delta\dot{\theta}_x \\ \Delta\dot{\theta}_y \end{Bmatrix}$$

$$+ \begin{bmatrix} K_{xx} & K_{xy} & K_{x\theta_x} & K_{x\theta_y} \\ K_{yx} & K_{yy} & K_{y\theta_x} & K_{y\theta_y} \\ K_{\theta_{x}x} & K_{\theta_{x}y} & K_{\theta_{x}\theta_{x}} & K_{\theta_{x}\theta_{y}} \\ K_{\theta_{y}x} & K_{\theta_{y}y} & K_{\theta_{y}\theta_{x}} & K_{\theta_{y}\theta_{y}} \end{bmatrix}\begin{Bmatrix} \Delta x \\ \Delta y \\ \Delta_x \\ \Delta_y \end{Bmatrix} = \begin{Bmatrix} 0 \\ 0 \\ 0 \\ 0 \end{Bmatrix} \qquad (3.5)$$

Considering translational motion in z-direction and rotational motion in θ_x, θ_y-direction, the linearized dynamic equation of thrust bearing is as Eqn. (2.21)
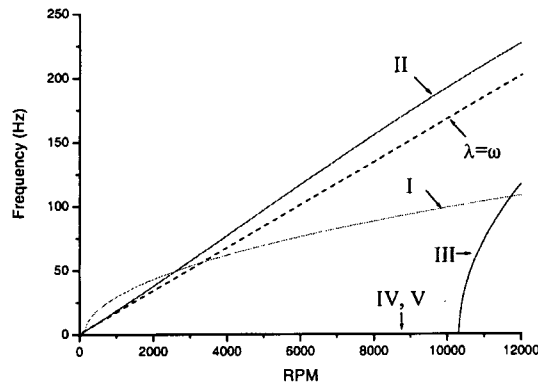
Assuming that no external force is applied to the system with the steady-state conditions, Eqn. (2.21) will be recast as following:
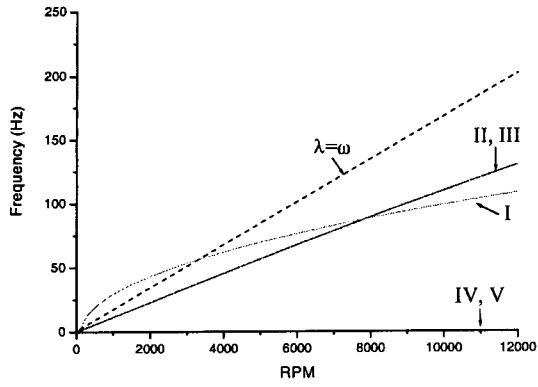
(a) Natural frequencies of the system at $\varepsilon = 0.0$

(b) Natural frequencies of the system at $\varepsilon = 0.4$
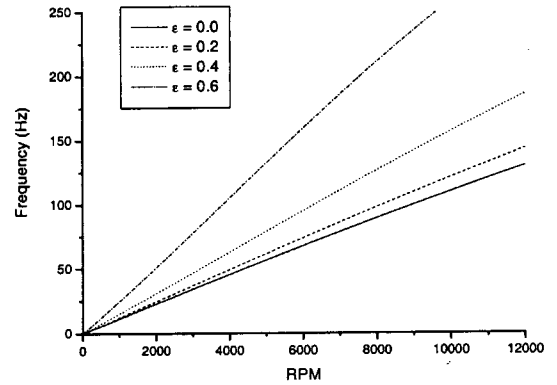

(c) Natural frequencies of the system at $\varepsilon = 0.5$

Fig. 8. Comparison of the natural frequencies for the effect of eccentricity ratio (ε).

Table 1. Characteristics of natural frequencies

Number of Mode	Principle Motion
I	Translational motion in z-direction
II	Translational motion in x,y-direction
III	Translational motion in x,y-direction + Rotational motion in θ_x, θ_y-direction
IV	Rotational motion in θ_x, θ_y-direction
V	Rotational motion in θ_x, θ_y-direction

(a) Variations of mode II for eccentricity ratio (ε)

(b) Variations of mode III for eccentricity ratio (ε)

Fig. 9. Comparison of the natural frequencies for the effect of eccentricity ratio (ε).

following:

$$\begin{bmatrix} M & 0 & 0 \\ 0 & Ixx & 0 \\ 0 & 0 & Iyy \end{bmatrix} \begin{Bmatrix} \Delta \ddot{z} \\ \Delta \ddot{\theta}_x \\ \Delta \ddot{\theta}_y \end{Bmatrix} + \begin{bmatrix} K_{zz} & K_{z\theta_x} & K_{z\theta_y} \\ K_{\theta_x z} & K_{\theta_x \theta_x} & K_{\theta_x \theta_y} \\ K_{\theta_y z} & K_{\theta_y \theta_x} & K_{\theta_y \theta_y} \end{bmatrix} \begin{Bmatrix} \Delta z \\ \Delta_x \\ \Delta_y \end{Bmatrix}$$

$$+ \begin{bmatrix} C_{zz} & C_{z\theta_x} & C_{z\theta_y} \\ C_{\theta_x z} & C_{\theta_x \theta_x} & C_{\theta_x \theta_y} \\ C_{\theta_y z} & C_{\theta_y \theta_x} & C_{\theta_y \theta_y} \end{bmatrix} \begin{Bmatrix} \Delta \dot{z} \\ \Delta \dot{\theta}_x \\ \Delta \dot{\theta}_y \end{Bmatrix} = \begin{Bmatrix} 0 \\ 0 \\ 0 \end{Bmatrix} \quad (3.6)$$

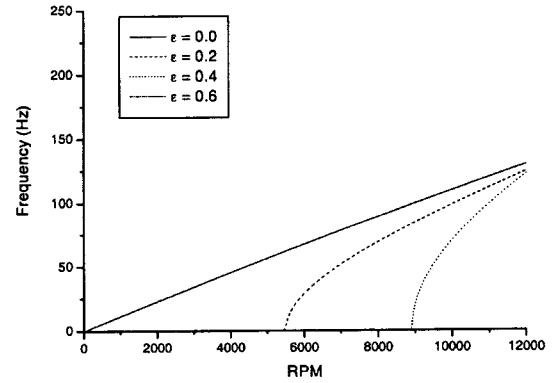Two of Eqn. (3.5) are for journal bearings and two of Eqn. (3.6) are for thrust bearings are added into one equation as

$$[M] \begin{Bmatrix} \Delta \ddot{x} \\ \Delta \ddot{y} \\ \Delta \ddot{z} \\ \Delta \ddot{\theta}_x \\ \Delta \ddot{\theta}_y \end{Bmatrix} + [K] \begin{Bmatrix} \Delta x \\ \Delta y \\ \Delta z \\ \Delta \theta_x \\ \Delta \theta_y \end{Bmatrix} + [C] \begin{Bmatrix} \Delta \dot{x} \\ \Delta \dot{y} \\ \Delta \dot{z} \\ \Delta \dot{\theta}_x \\ \Delta \dot{\theta}_y \end{Bmatrix} = \begin{Bmatrix} 0 \\ 0 \\ 0 \\ 0 \\ 0 \end{Bmatrix} \quad (3.7)$$

Eigen analysis is conducted to investigate the stability of the spindle bearing system. For the sake of computational purposes, Eqn. (3.7) is written in the first-order vector form as follows:
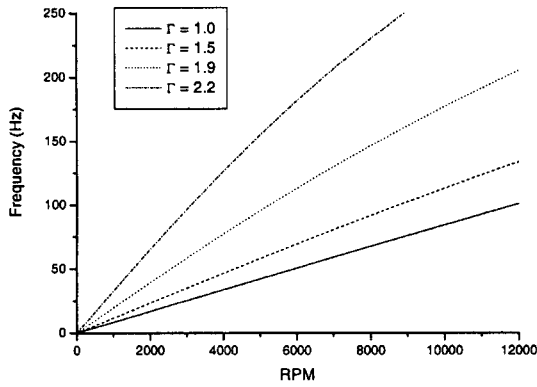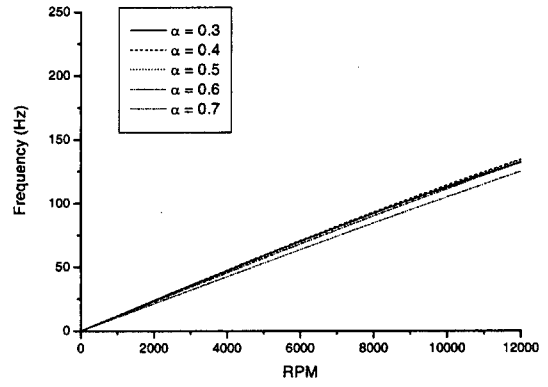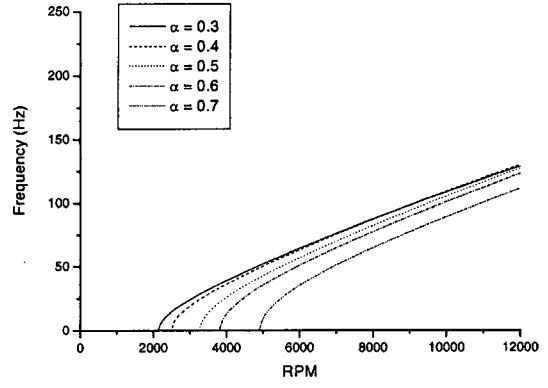
(a) Variations of mode □ for depth ratio (Γ)
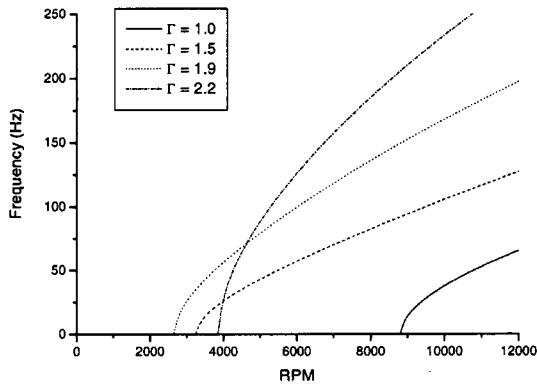
(b) Variations of mode □ for depth ratio (Γ)

Fig. 10 Comparison of the natural frequencies for the effect of depth ratio (Γ).

(a) Variations of mode Ⅱ for width ratio (α)

(b) Variations of mode □ for width ratio (α)

Fig. 11. Comparison of the natural frequencies for the effect of width ratio (α).

$$\begin{bmatrix} 0 & I \\ -M^{-1}K & -M^{-1}C \end{bmatrix}\begin{bmatrix} x \\ \dot{x} \end{bmatrix} = \begin{bmatrix} \dot{x} \\ \ddot{x} \end{bmatrix}$$ (3.8)

$$AP = \dot{P}, \quad P = qe^{\lambda t}$$

$$Aq = \lambda q$$

$$A = \begin{bmatrix} 0 & I \\ -M^{-1}K & -M^{-1}C \end{bmatrix}$$

Eigenvalue is obtained from the matrix , and the imaginary part of the eigenvalue is natural frequency of the system. When the system includes the fluid film bearing, the natural frequency of the system depends on the rotational speed. The stability of the system can be estimated by Campbell diagram in which the rotational speed as system input and the natural frequency as system output are displayed. Generally, horizontal axis is the rotational speed(RPM), and vertical axis is the natural frequency in Campbell diagram.

It shows the variations of natural frequency when eccentricity ratio changes in Fig. 8. There are five natural frequencies, but only the three natural frequencies show in Fig. 8 (b). Two natural frequencies go with x-axis because they are nil due to the presence of the bearing damping. After numbering the natural frequencies, modes of natural frequencies are investigated by the analysis of eigenvector. The
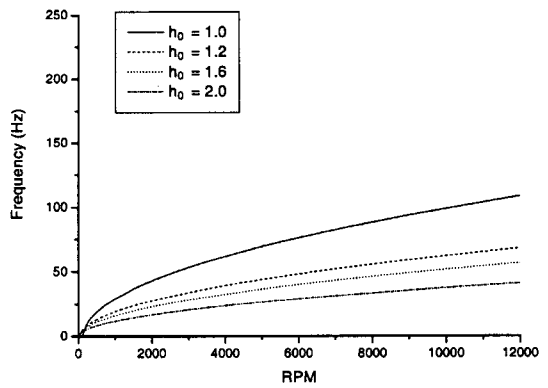

Fig. 12. Comparison of mode ? for the effect of clearance of thrust bearing.

results are arranged in Table 1.

It refers to a critical speed when the dashed line has an intersection with natural frequencies. Critical speed depends not only on the geometry of the bearing but also on the running condition. It maybe differs what kind of modes crossed with. In Fig. 8 (a), mode I meets the line ($\lambda = \omega$) around 3500 rpm, it means a critical speed. Besides, slope of mode Ⅱ increases with eccentricity ratio, and goes by the dashed line ($\lambda = \omega$) in Fig. 8 (b), (c). It means that there is a point when mode Ⅱ may goes with the dashed line ($\lambda = \omega$) in $\varepsilon = 0.5{\sim}0.6$, so it could be very unstable regardless of rotational speed. Then it is

necessary to compare the same mode of natural frequency for the parametric analysis.

Fig. 9 shows that mode II goes steeper as eccentricity ratio increases, it means that the whirl ratio of journal bearing increases. Mode III appears from higher speed and goes steeper as eccentricity ratio increases. At large eccentricity ratio, mode III will meets the dashed line ($\lambda = \omega$) to make another critical speed beyond 12,000 rpm. Besides, mode I does not change with the variation of eccentricity ratio.

In Fig. 10, it shows that how each mode changes for the variation of groove depth ratio. Mode III starts at lower rpm with the increment of groove depth ratio up to $\Gamma = 1.9$, but after that region, it starts at larger rpm. And inclination is proportional to the groove depth ratio.

As the groove width ratio increases, mode III starts at higher rpm in the same shape. On the other hand, mode I and II change little as shown in Fig. 11. It means that mode III can be shifted by groove width ratio.

In Fig. 12, only mode I changes with the variation of thrust bearing clearance. As the clearance increases, stiffness coefficients and damping coefficients decrease so that natural frequency diminishes. Critical speed resulted from mode I is avoidable by adjusting of the clearance on condition that the load carrying capacity of the thrust bearing is sufficient.

Conclusion

Herringbone groove journal bearing and spiral groove thrust bearing are modeled separately to analyze the characteristics of the spindle motor bearing which is composed of these two bearing. The Reynolds equation is solved for static and dynamic characteristics with perturbation method. Not only translational motion but also two degrees of freedom rotational motion are considered to simulate the actual motion. Several geometric parameters of journal and thrust bearings are numerically analyzed to investigate the characteristics of bearings. Then spindle motor bearing composed of two herringbone groove journal bearings and two thrust bearings is modeled as a whole and solved numerically. Bearing instability can be estimated through the eigen analysis and can be possible to avoid by the adjusting geometric parameters and operating conditions.

Acknowledgment

References

1. Bonneau, D. and Absi, J., 1994, Analysis of Aerodynamic Journal Bearings with Small Number of Herringbone Grooves by Finite Element Method, ASME Journal of Tribology, Vol. 116, pp. 698-704.
2. Kang, K., Rhim, Y. and Sung, K., 1996 A Study of the Oil-Lubricated Herringbone Grooved Journal Bearing- Part 1:Numerical Analysis, ASME Journal of Tribology Vol. 118 pp.906-911
3. Qiu, Z. L. and Tieu, A. K., Misalignment Effect on the Static and Dynamic Characteristics of Hydrodynamic Journal Bearings, 1995, ASME Journal of Tribology, V.117 pp. 717-723
4. Yan Zan and Michael R. Hatch, Calculation of Dynamic Characteristics of Coupled Herringbone Journal and Thrust Hydrodynamic Bearing, 1996, Adv. Info. Storage Syst. Vol. 7, pp. 115-126
5. Yan Zan and Michael R. Hatch, On the Whirl Dynamics of the Hydrodynamic Bearing Spindle in Information Storage Systems, 1996, International Symposium on Information Storage and Processing Systems, Vol. 2, pp. 73-84
6. Rahman, M., Leuthold, H., Computer Simulation of a Coupled Journal and Thrust Hydrodynamic Bearing using a Finite-Element Method, 1996, IMCSD Proceedings, pp. 103-112
7. Jiasheng Zhu and Kyosuke Ono A Comparison Study on the Performance of Four Types of Oil Lubricated Hydrodynamic Thrust Bearings for Hard Disk Spindles, 1999, ASME Journal of Tribology, V.121 pp. 114-120 N.1
8. Jang, G. H., Kim Y. J., Calculation of dynamic coefficients in a hydrodynamic bearing considering five degrees of freedom for a general rotor-bearing system, 1999, ASME Journal of Tribology, Vol.121, pp. 499-505 N.3
9. Kawabata, N., Ozawa, Y., Kamaya, S., and Miyake, Y., Static Characteristics of the Regular and Reversible Rotation Type Herringbone Grooved Journal Bearing, 1989, ASME Journal of Tribology, Vol. 111, pp. 484-490.
10. Lalanne, M., Ferraris, G., Rotordynamics Prediction in Engineering, 1990, John Wiley & Sons
11. Vance, J., M., Rotordynamics of Turbomachinery, 1988, John Wiley & Sons
12. Friswell, M. I., Garvey, S. D., Penny, J. E. T., Smart, M. G., Computing Critical Speeds for Rotating Machines with Speed Dependent Bearing Properties, 1998, ASME Journal of Sound and Vibration, Vol. 213, pp. 139-158